Asymmetrically Clipped Optical Hadamard Coded Modulation (ACO-HCM)

Henrik Schulze , *Member, IEEE*, and Peter A. Hoeher , *Fellow, IEEE*

Abstract—In many optical wireless communications systems, power efficiency is paramount. In others, flexibility is important. To achieve these goals, this paper presents a novel transmission scheme dubbed *asymmetrically clipped optical Hadamard coded modulation (ACO-HCM)*. ACO-HCM combines the characteristics of real-valued non-negative orthogonal frequency-division multiplexing (OFDM) and Hadamard coded modulation (HCM). Unlike OFDM, which is based on the Fourier transform and therefore delivers a continuous waveform, ACO-HCM provides a discrete set of amplitudes. This feature is desirable for nonlinear channels. Error probabilities are analytically calculated for a linear receiver similar to the decorrelation receiver in direct-sequence code-division multiple access (DS-CDMA). Maximum-likelihood sequence estimation is also investigated and shown to outperform the linear receiver, particularly in the presence of a time-dispersive channel. The peak-to-average power ratio of ACO-HCM is derived for the electrical as well as the optical domain in closed form.

Index Terms—Error analysis, Hadamard transform, intensity modulation, OFDM modulation, optical wireless communication, visible light communication.

I. INTRODUCTION

IN OPTICAL wireless communication, a distinction is made between lasers and light-emitting diodes (LEDs). Lasers are often used in free space optical (FSO) systems, while LEDs are often employed indoors. Since lasers are capable of generating coherent light waves, two-dimensional (i.e., complex-valued) modulation techniques can be used in conjunction with a coherent detector. Conversely, LEDs provide incoherent light, i.e. the phase is not useful for data transmission. The most simple modulation/detection strategy suitable for lasers and LEDs, respectively, is intensity modulation with direct detection (IM/DD). Regarding LED-based IM/DD, infrared (IR) communication has traditionally been studied [1], [2]. Recent interest is in visible light communication (VLC) and in visible light positioning (VLP) [3], [4], [5], [6]. Among the benefits of optical IM/DD communication systems are: Tremendous unregulated bandwidth, no frequency planning due to limited coverage area, electromagnetic compatibility and interference immunity, data security on the physical layer, license-free operation, high area

spectral efficiency, cheap optical devices, and energy efficiency in joint illumination and communication scenarios [6].

IM/DD waveforms must be real-valued and non-negative. It is advantageous to use signals with high amplitude fluctuations, because for a given optical transmit power, the electrical power at the receiver is higher compared to signals with low amplitude fluctuations [7].

Orthogonal frequency-division multiplexing (OFDM) is suitable for incoherent optical transmission, since OFDM signals are characterized by high amplitude fluctuations (besides providing beneficial features like single-tap equalization in conjunction with a cyclic prefix and high spectral efficiency in combination with high-order modulation schemes). However, due to the aforementioned signal limitations, OFDM techniques cannot be applied directly. In addition to simply adding a DC offset either in the analog domain by a bias-T or in the digital domain, known as DC-offset OFDM (DCO-OFDM) [8], [9], techniques have been developed to put a constraint on the OFDM signal. This constraint makes the negative part of the waveform redundant, and hence allows to clip its negative parts without information loss by the clipping. Asymmetrically clipped optical OFDM (ACO-OFDM) [10], [11], pulse amplitude modulation with digital multitone transmission (PAM-DMT) [12], and flipped OFDM (Flip-OFDM) [13] are three quite similar, frequently used variants of OFDM. They offer a significant performance gain compared to conventional on-off keying (OOK) with non-return-to-zero (NRZ) pulses [14].

However, because Fourier transform-based OFDM techniques produce continuous waveforms with high amplitude fluctuations, they are very sensitive to non-linearities. In contrast, a modulation scheme that utilizes only a discrete set of signal amplitudes is favorable for implementation, because it can be realized by a set of different LEDs that are just switched on or off. Effectively, the linearity of the transmitter is achieved by implementing a superposition of the individual signals in the medium. Hadamard coded modulation HCM [15], [16], [17] is such a scheme. But in the absence of nonlinearities, HCM has a worse error performance compared to amplitude shift keying (ASK) that is mimicked by separate light sources [7].

In this paper, we present a novel modulation scheme dubbed *asymmetrically clipped optical Hadamard coded modulation (ACO-HCM)*. This modulation scheme combines the performance benefits of the unipolar OFDM techniques mentioned above, with the benefits of HCM utilizing a discrete signal range. It is shown that the constraints making the negative part of the signal redundant can be transferred from the Fourier transform

to the Hadamard transform, also known as the Walsh-Hadamard transform (WHT).

The main contributions of this paper and features of this novel modulation technique are:

- The concept of ACO-OFDM and PAM-DMT is transferred to Hadamard matrices.
- Sinusoids are replaced by Walsh-Hadamard sequences and negative amplitudes are clipped in order to obtain unipolar signals defined over a discrete set of amplitude values.
- A possible implementation consists of superimposing the light of a set of LEDs, which are only switched on and off.
- A linear receiver based on a partial Hadamard back transform is proposed.
- Semi-analytic and simulated bit error rates are presented for the linear receiver and a maximum-likelihood receiver for noisy channels without and with time-dispersion.

The remainder of this paper is organized as follows. The proposed ACO-HCM transmission scheme is introduced in Section II. In Section III, an error probability performance analysis of ACO-HCM based on the linear receiver is provided for the electrical domain and the optical domain assuming additive white Gaussian noise (AWGN). Performance improvements by using a maximum-likelihood receiver are investigated in Section IV. Afterwards, bit error rate (BER) simulations are provided in Section V. In Section VI, the performance analysis and BER evaluation are expanded to the time-dispersive channel. Possible extensions of ACO-HCM are suggested in Section VII. Finally, conclusions are drawn in Section VIII.

II. THE TRANSMISSION SETUP

A. Some Relevant Properties of Hadamard Matrices

Let $\mathbf{H}$ be the (bipolar) $N \times N$ Hadamard matrix, where $N > 1$ is a power of two. As an example, the Hadamard matrix for $N = 8$ is given by

$$\mathbf{H} = \begin{pmatrix} 1 & 1 & 1 & 1 & 1 & 1 & 1 & 1 \\ 1 & -1 & 1 & -1 & 1 & -1 & 1 & -1 \\ 1 & 1 & -1 & -1 & 1 & 1 & -1 & -1 \\ 1 & -1 & -1 & 1 & 1 & -1 & -1 & 1 \\ 1 & 1 & 1 & 1 & -1 & -1 & -1 & -1 \\ 1 & -1 & 1 & -1 & -1 & 1 & -1 & 1 \\ 1 & 1 & -1 & -1 & -1 & -1 & 1 & 1 \\ 1 & -1 & -1 & 1 & -1 & 1 & 1 & -1 \end{pmatrix}. \quad (1)$$

We denote the column vectors by $\mathbf{h}_n$ and express the matrix as

$$\mathbf{H} = (\mathbf{h}_1, \mathbf{h}_2, \ldots, \mathbf{h}_N) \quad (2)$$

and its elements as

$$h_{mn} = h_n[m] \quad (3)$$

with $m, n = 1, \ldots, N$. We say that $\mathbf{h}_n$ is a column vector of *even symmetry*, if

$$h_n[m] = h_n[N - (m - 1)], \quad (4)$$

i.e., the first element equals the last one, the second element equals the second to last, and so on. We say that $\mathbf{h}_n$ is a column

vector of *odd symmetry*, if

$$h_n[m] = -h_n[N - (m - 1)], \quad (5)$$

i.e., the first row of $\mathbf{G}$ is equal to the negated last row, the second row is equal to the negated penultimate row, and so on. We notice that half of the columns of the Hadamard matrix are of even and the others are of odd symmetry. This follows from the recursive construction scheme of the $2N \times 2N$ Hadamard matrix $\mathbf{H}^{(2N)}$ from the $N \times N$ Hadamard matrix $\mathbf{H}^{(N)}$ according to

$$\mathbf{H}^{(2N)} = \begin{pmatrix} \mathbf{H}^{(N)} & \mathbf{H}^{(N)} \\ \mathbf{H}^{(N)} & -\mathbf{H}^{(N)} \end{pmatrix} \quad (6)$$

with the initialization

$$\mathbf{H}^{(2)} = \begin{pmatrix} 1 & 1 \\ 1 & -1 \end{pmatrix}. \quad (7)$$

Let $\mathbf{h}_n^{(N)}$ be a column vector of $\mathbf{H}^{(N)}$. According to the construction, the first N column vectors of $\mathbf{H}^{(2N)}$ are obtained as

$$\mathbf{h}_n^{(2N)} = \begin{pmatrix} \mathbf{h}_n^{(N)} \\ \mathbf{h}_n^{(N)} \end{pmatrix}, \quad (8)$$

and the last N column vectors of $\mathbf{H}^{(2N)}$ are yielded as

$$\mathbf{h}_{n+N}^{(2N)} = \begin{pmatrix} \mathbf{h}_n^{(N)} \\ -\mathbf{h}_n^{(N)} \end{pmatrix}. \quad (9)$$

We further observe (and can prove by simple index calculations) that for the first N vectors the symmetry is retained and for the last N vectors the symmetry is inverted. Furthermore, the symmetry of a column vector can equivalently be characterized by the sign of its last element: A positive sign indicates even symmetry, while a minus sign indicates odd symmetry. Writing $+$ for even and $-$ for odd symmetry, we find the following scheme for the first Hadamard matrices:

$$\begin{array}{llllllllll} N = 2 & : & + & - \\ N = 4 & : & + & - & - & + \\ N = 8 & : & + & - & - & + & - & + & + & - \end{array}$$

B. ACO-HCM Signal Generation

We write $\mathbf{H}^{(o)}$ for the $N \times N/2$ matrix obtained from $\mathbf{H}$ by deleting the $N/2$ columns of even symmetry and keeping the $N/2$ columns of odd symmetry. For $N = 8$, this leads to

$$\mathbf{H}^{(o)} = \begin{pmatrix} 1 & 1 & 1 & 1 \\ -1 & 1 & 1 & -1 \\ 1 & -1 & 1 & -1 \\ -1 & -1 & 1 & 1 \\ 1 & 1 & -1 & -1 \\ -1 & 1 & -1 & 1 \\ 1 & -1 & -1 & 1 \\ -1 & -1 & -1 & -1 \end{pmatrix}. \quad (10)$$

For the further analysis, it is convenient to use the matrix

$$\mathbf{G} = \frac{1}{\sqrt{N}} \mathbf{H}^{(o)} \quad (11)$$

Fig. 1. Block diagram of the ACO-HCM signal generator.

with normalized column vectors. This matrix describes an *isometry*, i.e. it leaves scalar products invariant because of the property

$$\mathbf{G}^\mathsf{T}\mathbf{G} = \mathbf{I}_{N/2}, \tag{12}$$

where $\mathbf{I}_{N/2}$ is the $N/2 \times N/2$ identity matrix. We denote the matrix elements of $\mathbf{G}$ as g_{mn} with $m = 1, \ldots, N$ and $n = 1, \ldots, N/2$.

Now let $\mathbf{u}$ be a column vector of length $N/2$ whose elements are M-PAM symbols $u_n \in \{\pm\delta, \pm3\delta, \ldots, \pm(M-1)\delta\}$, where δ is the Euclidean half distance inside the constellation. The *generator matrix* $\mathbf{G}$ maps an $N/2$-dimensional symbol vector to an N-dimensional signal vector

$$\mathbf{x} = \mathbf{G}\mathbf{u} \tag{13}$$

with elements

$$x_m = \sum_{n=1}^{N/2} g_{mn}u_n. \tag{14}$$

In (13) corresponds to a rate-1/2 block code. Thanks to the isometry given by (12), the data vector $\mathbf{u}$ can be recovered from $\mathbf{x}$ as

$$\mathbf{u} = \mathbf{G}^\mathsf{T}\mathbf{x}, \quad \text{i.e.,} \quad u_n = \sum_{m=1}^{N} g_{mn}x_m \tag{15}$$

by applying the partial Hadamard back transform described by the matrix $\mathbf{G}^\mathsf{T}$. Since the column vectors of $\mathbf{G}$ have odd symmetry, the vector $\mathbf{x}$ also has odd symmetry, that is

$$x_m = -x_{N-(m-1)}, \tag{16}$$

because $\mathbf{x}$ is a superposition of these column vectors. The negative part of a signal vector with odd symmetry is redundant. Thus, this part may be clipped without information loss. This also holds for ACO-OFDM [10] and PAM-DMT [12]. By making the signal ready for clipping, half of the possible data rate is sacrificed.

We define the clipped signal vector $\mathbf{x}^{(+)}$ by its elements

$$x_m^{(+)} = \sqrt{2}\,\Theta(x_m)x_m, \tag{17}$$

where $\Theta(x)$ is the Heaviside step function. The factor $\sqrt{2}$ has been introduced to renormalize the energy after clipping. The ACO-HCM signal generation is depicted in Fig. 1. A bit vector $\mathbf{b}$ of length $\log_2(M) \cdot N/2$ is mapped to a length-$N/2$ PAM symbol vector $\mathbf{u}$. This vector $\mathbf{u}$ is mapped to a length-N signal vector $\mathbf{x}$. The elements of this signal vector are denoted as *chips*. Clipping the negative chips leads to the final signal vector $\mathbf{x}^{(+)}$.

The computational complexity of ACO-HCM signal generation is $O(N \log_2 N)$ for $N/2$ data symbols, i.e. $O(\log_2 N)$ per symbol. The calculations are integer and not complex-valued as in ACO-OFDM. For reasonably small N, the WHT can even be avoided by a lookup table.

C. Some ACO-HCM Signal Properties

From (14) and (17) it follows that $x_m^{(+)}$ takes values between zero and

$$x_\mathsf{max}^{(+)} = (M-1)\sqrt{\frac{N}{2}}\delta. \tag{18}$$

We further note that due to the isometry (12) and the normalization included in the clipping, all vectors have the same energy

$$\|\mathbf{u}\|^2 = \|\mathbf{x}\|^2 = \left\|\mathbf{x}^{(+)}\right\|^2. \tag{19}$$

We also note that $E_\mathsf{s} = \mathrm{E}\{u_n^2\}$ is the average energy per PAM symbol and $E_\mathsf{b} = E_\mathsf{s}/\log_2(M)$ is the average energy per bit, where $\mathrm{E}\{\cdot\}$ denotes the expectation. Since the $N\log_2(M)/2$ bits are mapped to N chips, the bit rate R_b is related to the chip rate R_c by $R_\mathsf{b} = \frac{1}{2}\log_2(M)R_\mathsf{c}$.

As shown in Appendix A, the peak-to-average power ratio (PAPR) of ACO-HCM can be derived for the electrical domain as

$$\mathsf{PAPR}_\mathsf{el} = \frac{\left(x_\mathsf{max}^{(+)}\right)^2}{\mathrm{E}\left\{\left(x_i^{(+)}\right)^2\right\}} = 3N\frac{M-1}{M+1}, \tag{20}$$

briefly called *electrical PAPR*.

The properties of the ACO-HCM signal allow a simple linear receiver very similar to the one for ACO-OFDM. For this purpose, we define the odd symmetry Hadamard coefficients $u_n^{(+)}$ and the corresponding vector $\mathbf{u}^{(+)}$ of the clipped signal by

$$u_n^{(+)} = \sum_{m=1}^{N} g_{mn}x_m^{(+)}, \quad \text{i.e.,} \quad \mathbf{u}^{(+)} = \mathbf{G}^\mathsf{T}\mathbf{x}^{(+)}. \tag{21}$$

One can prove the following

Theorem 1: The coefficients $u_n^{(+)}$ of the clipped signal $x_m^{(+)}$ defined by (21) are related to the original PAM symbols u_n by

$$u_n^{(+)} = \frac{1}{\sqrt{2}}u_n. \tag{22}$$

The proof is provided in Appendix B.

III. ACO-HCM PERFORMANCE ANALYSIS FOR THE LINEAR RECEIVER

In this section, we restrict ourselves to an AWGN channel and ignore time-dispersion. Regarding the noise statistics, LEDs are assumed throughout the paper. Furthermore, we assume an average power normalization rather than a peak-power limitation.

A. Electrical Domain

We begin by considering an N-dimensional discrete real-valued AWGN channel with noise vector $\mathbf{m}$ of variance $N_0/2$ in each dimension. Accordingly, the receive (Rx) vector is

$$\mathbf{y} = \mathbf{x}^{(+)} + \mathbf{m}. \tag{23}$$

The corresponding linear ACO-HCM receiver is depicted in Fig. 2. Applying the detector matrix $\mathbf{G}^\mathsf{T}$ at the receiver yields
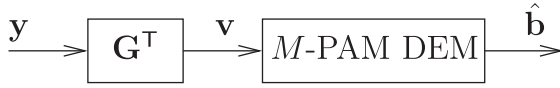
Fig. 2. Block diagram of the linear ACO-HCM receiver.

the vector

$$\mathbf{G}^{\mathsf{T}}\mathbf{y} = \mathbf{G}^{\mathsf{T}}\mathbf{x}^{(+)} + \mathbf{G}^{\mathsf{T}}\mathbf{m}. \tag{24}$$

Noting that the transformed vector $\mathbf{n} = \mathbf{G}^{\mathsf{T}}\mathbf{m}$ is an $N/2$-dimensional white Gaussian noise vector of the same variance $N_0/2$ in each dimension and using (21) and (22), we can write

$$\mathbf{v} = \frac{1}{\sqrt{2}}\mathbf{u} + \mathbf{n} \tag{25}$$

for the vector $\mathbf{v} = \mathbf{G}^{\mathsf{T}}\mathbf{y}$. This means that the partial Hadamard back transform $\mathbf{G}^{\mathsf{T}}$ yields an equivalent AWGN channel for the PAM symbol vector $\mathbf{u}$, but with a power loss of a factor two that is caused by the clipping. The same property is known from ACO-OFDM [10] and PAM-DMT [12].

The error event probability for real-valued baseband M-PAM can be written as

$$P_{\text{error}} = \frac{1}{2}\text{erfc}\left(\sqrt{\gamma \frac{E_\mathsf{b}}{N_0}}\right) \tag{26}$$

with γ given by [18]

$$\gamma_{\text{PAM}} = \frac{3\log_2 M}{M^2 - 1}. \tag{27}$$

For ACO-HCM, due to the power loss mentioned above, (27) has to be replaced by

$$\gamma_{\text{ACO}} = \frac{3}{2}\frac{\log_2 M}{M^2 - 1}. \tag{28}$$

The constant γ in (26) can be interpreted as the *power efficiency factor* of the constellation because the bit energy $E_\mathsf{b} = P_\mathsf{s}/R_\mathsf{b}$ is the (electrical) signal power P_s per bit rate R_b that is needed to achieve a certain error rate. The signal-to-noise-ratio (SNR) is given as

$$\text{SNR} = \frac{P_\mathsf{s}}{N_0 B_\mathsf{n}}, \tag{29}$$

where B_n is the noise bandwidth and can be related to E_b/N_0 by

$$\text{SNR} = \frac{R_\mathsf{b}}{B_\mathsf{n}}\frac{E_\mathsf{b}}{N_0}. \tag{30}$$

B. Optical Domain

For the optical channel, the error probability has to be expressed by the average optical power Φ, sometimes also denoted as P_{opt}. For an AWGN channel, the photocurrent at the receiver is given by

$$y(t) = x(t) + n(t), \tag{31}$$

where $x(t)$ is the useful signal and $n(t)$ is a white Gaussian noise process defined by the autocorrelation

$$\text{E}\{n(t)n(t')\} = \frac{N_\mathsf{i}}{2}\delta(t - t'). \tag{32}$$

Since all analogue signals are currents, the one-sided spectral density of the noise current, N_i, has dimension $[N_\mathsf{i}] = \text{A}^2/\text{Hz}$. The noise is typically modeled as a superposition of shot noise and thermal noise components, see e.g. [2]. The shot noise is assumed to be dominated by ambient light, i.e. largely data-independent. Then, the electrical SNR can be expressed as

$$\text{SNR} = \frac{\text{E}\{x^2(t)\}}{N_\mathsf{i}B_\mathsf{n}}, \tag{33}$$

where B_n is the noise bandwidth. The photocurrent corresponding to the useful signal is given by $x(t) = r\,\phi(t)$, where r is the responsivity of the photodetector, and $\phi(t)$ is the time-varying power of the received optical signal with average power denoted by $\Phi = \text{E}\{\phi(t)\}$. This optical power has to be related to the quantity $\text{E}\{x^2(t)\}$, which is proportional to the electrical power and determines the bit error rate. In order to do this, we introduce the *shaping gain factor*

$$\kappa \triangleq \frac{\text{E}\{x^2(t)\}}{\text{E}\{x(t)\}^2} \tag{34}$$

and find that the electrical SNR can be written as

$$\text{SNR} = \kappa \frac{(r\,\Phi)^2}{N_\mathsf{i}B_\mathsf{n}}. \tag{35}$$

Since the BER is a function of the SNR and the SNR depends on κ, the BER performance for the optical channel is influenced by the shape of the signal. This is in contrast to the electrical radio channel where – for the matched filter receiver and ideal synchronization – the performance is independent of the pulse shape. Comparing (30) and (35) we find

$$\frac{E_\mathsf{b}}{N_0} = \kappa \frac{(r\,\Phi)^2}{N_\mathsf{i}R_\mathsf{b}}, \tag{36}$$

and the error event probability of (26) can be expressed by the average optical power as

$$P_{\text{error}} = \frac{1}{2}\text{erfc}\left(\sqrt{\gamma\kappa\frac{(r\,\Phi)^2}{N_\mathsf{i}R_\mathsf{b}}}\right). \tag{37}$$

For a pulse train

$$x(t) = \sum_i x_i\,g(t - i\,T) \tag{38}$$

of symbols x_i with rate $1/T$, the shaping gain factor κ depends on the shape of the pulse $g(t)$. In this paper, for simplicity, we assume rectangular pulses. In this case, the shaping gain factor is simply given by

$$\kappa = \frac{\text{E}\{x_i^2\}}{\text{E}\{x_i\}^2}. \tag{39}$$

For ACO-HCM, the symbols x_i in (38) and (39) have to be understood as the clipped symbols $x_i^{(+)}$.

TABLE I
NUMERICALLY EVALUATED VALUES FOR κ

N	κ (2-PAM)	κ (4-PAM)	κ (8-PAM)	κ (16-PAM)
4	4	3.204	3.052	3.012
8	3.556	3.142	3.083	3.070
16	3.344	3.146	3.116	3.104
32	3.241	3.144	3.129	3.122
64	3.191	3.142	3.135	3.131
128	3.166	3.141	3.139	3.136
256	3.154	3.142	3.140	3.139

As a consequence of the structure of the generator matrix $\mathbf{G}$, each symbol x_m in (14) results from a random walk of length $L = N/2$. For large L, according to the central limit theorem (CLT), we expect a zero-mean Gaussian probability density function (PDF) with variance σ^2 for the unclipped signal. Clipping the negative values leads to the following PDF for the signal:

$$p(x) = \frac{1}{2}\delta(x) + \frac{1}{\sqrt{2\pi}\sigma}\exp\left(-\frac{1}{2\sigma^2}x^2\right)\Theta(x). \qquad (40)$$

Given this PDF, we get $\mathrm{E}\{x\} = \sigma/\sqrt{2\pi}$ and $\mathrm{E}\{x^2\} = \sigma^2/2$, which leads to $\kappa = \pi$. The optical power efficiency factor is then given by

$$\gamma\kappa = \frac{\pi}{2}\gamma_{M\text{-PAM}}. \qquad (41)$$

We see that the shaping gain factor $\kappa = \pi$ overcompensates the power loss of $1/2$ due to the clipping by the factor $\pi/2 \approx 1.57 \approx 2\,\mathrm{dB}$. Thus, for 2-PAM modulation in each real-valued dimension with $\gamma_{2\text{-PAM}} = 1$ and large L, ACO-HCM offers a 2 dB gain compared to the reference scheme OOK with

$$P_{\text{error,OOK}} = \frac{1}{2}\mathrm{erfc}\left(\sqrt{\frac{(r\,\Phi)^2}{N_{\mathrm{i}}R_{\mathrm{b}}}}\right), \qquad (42)$$

see [1, (5.15)], which means $(\gamma\kappa)_{\text{OOK}} = 1$. (Note the different definition of N_{i} by a factor of two in [1].) Hence, $\gamma\kappa$ is the gain compared to this reference scheme. In practice, L may be of moderate size so that the premise of the CLT may not exactly be fulfilled. However, the symbol statistics can be analyzed numerically. The results for 2-PAM and 4-PAM are shown in Table I. As expected, $\kappa \to \pi$ for large N. For 2-PAM, $\kappa > \pi$ holds for all values in the table so we might conjecture that the convergence is from above. This is not the case for higher values of M. However, $\kappa \approx \pi$ is either a good approximation or a conservative estimate for all values in the table.

The parameter κ has another interesting meaning. Let us define the PAPR in the *optical* domain as the ratio

$$\mathrm{PAPR}_{\text{opt}} = \frac{x_{\max}^{(+)}}{\mathrm{E}\left\{x_i^{(+)}\right\}} \qquad (43)$$

between the maximal and the average optical power. We thus obtain the general

Theorem 2: The optical PAPR in (43) is related to the electrical PAPR in (20) by the parameter κ according to

$$\mathrm{PAPR}_{\text{opt}}^2 = \kappa \cdot \mathrm{PAPR}_{\text{el}}. \qquad (44)$$

This simple but fundamental law holds for any optical IM/DD digital modulation scheme. A detailed derivation of the PAPR, the proof of the theorem, and a comparison with OOK is given in Appendix A.

A consequence of (34) is that the received powers in the optical and the electrical domain are related as [6]

$$P_{\text{el}} \propto \kappa \cdot P_{\text{opt}}^2. \qquad (45)$$

Consequently, for a given received optical power P_{opt}, the received power P_{el} in the electrical domain is boosted by $\kappa > 1$. This property is important for data detection, which takes place in the electrical domain. The shaping factor κ partly explains why return-to-zero (RZ) signals usually outperform NRZ signals in optical communications [19]. Note that precoding-type PAPR reduction techniques inherently reduce κ, since this parameter is a signal property. Hence, in OWC systems, precoding-type PAPR reduction techniques are counter-productive as long as nonlinear effects of the light source are avoidable. In ACO-HCM the latter constraint is indeed avoidable, because due to the discrete-valued waveform the light sources can be operated in parallel and hence each light source can be driven by a two-level switching signal. OFDM-based waveforms are continuous-valued, however, and hence there is a trade-off between the shaping gain κ and benefits from precoding-type PAPR reduction techniques. An in-depth investigation and optimization is suggested for optical modulation schemes with continuous-valued transmit signal in future work. In the area of radio communications, (45) is not applicable and precoding-type PAPR reduction seems to be beneficial in any cases. Examples include FFT-precoding [20] (which is applied in the 4 G LTE uplink) and WHT-precoding [21].

IV. IMPROVEMENTS BY USING AN MLSE RECEIVER

A. Analysis of the Clipping

Let us reconsider the 3 dB electrical power loss due to the factor $1/\sqrt{2}$ in (25), which is caused by the clipping. Recall that the generator matrix $\mathbf{G}$ maps a PAM signal vector $\mathbf{u}$ from the $N/2$ dimensional real-valued signal space to a vector $\mathbf{x} = \mathbf{Gu}$ inside the $N/2$ dimensional subspace span($\mathbf{G}$) of $\mathbb{R}^N$ that is spanned by the column vectors of $\mathbf{G}$. Because $\mathbf{G}$ is isometric, the signal energy $\|\mathbf{x}\|^2 = \|\mathbf{u}\|^2$ is retained. According to (19), the clipping operation $\mathbf{x} \mapsto \mathbf{x}^{(+)}$ retains the signal energy as well. The energy is not lost, it is somewhere else: Half of the energy moves from the $N/2$ dimensional subspace span($\mathbf{G}$) to the other $N/2$ dimensions in $\mathbb{R}^N$. To analyze this, let us define the normalized Hadamard base vectors

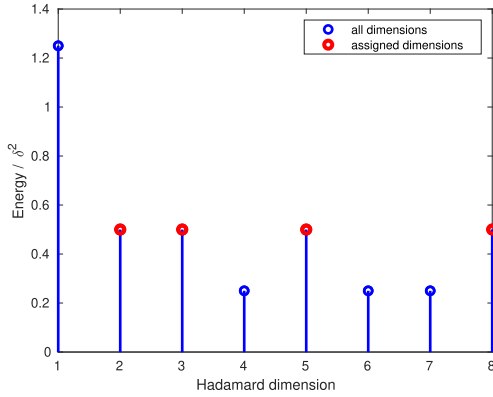$$\mathbf{f}_n = \frac{1}{\sqrt{N}}\mathbf{h}_n, \quad n = 1, \ldots, N, \qquad (46)$$

Fig. 3.   The Hadamard spectrum for $N = 8$ and 2-PAM.

that build an orthonormal base of $\mathbb{R}^N$. The ACO-HCM signal can be written as a superposition

$$\mathbf{x}^{(+)} = \sum_{n=1}^{N} c_n \mathbf{f}_n \tag{47}$$

of these base vector with coefficients given by the scalar products

$$c_n = \mathbf{f}_n \cdot \mathbf{x}^{(+)} \tag{48}$$

obtained from the (full) Hadamard back transform. These c_n can be called Hadamard coefficients. The total signal energy is given by

$$\left\| \mathbf{x}^{(+)} \right\|^2 = \sum_{i=1}^{N} c_n^2 , \tag{49}$$

and the contribution c_n^2 can be interpreted as the energy that is allocated to the dimension number n. We may thus speak of the Hadamard spectrum in analogy to the Fourier spectrum, which has the same interpretation. The numerically obtained Hadamard spectrum $\mathrm{E}\{c_n^2\}$ for $N = 8$ and a sufficiently large number of simulated 2-PAM symbols is depicted in Fig. 3. The values for the dimension numbers $n = 2, 3, 5, 8$ corresponding to base vectors of odd symmetry (i.e. the columns vectors of $\mathbf{G}$) are indicated by red circles. We observe that the energy in these assigned dimensions is reduced from δ^2 to $\delta^2/2$ due to the clipping, whilst the previously empty dimensions now carry energy. Thus, the effect of clipping is to move energy from the assigned dimensions to the others.

B. Optimal Receiver

From the above discussion, we conclude that the receiver of Fig. 2 cannot be optimal because it considers only the energy in the assigned dimensions of the odd symmetry base vectors and disregards the rest. The maximum-likelihood sequence estimation (MLSE) receiver takes into account all dimensions of the transmitted signal. We write $\mathbf{X}^{(+)}$ for the $N \times M^{N/2}$ matrix of all possible ACO-HCM transmit vectors $\mathbf{x}^{(+)}$. Under the above mentioned assumption of an AWGN channel without dispersion, the MLSE receiver chooses the vector closest to the given Rx

vector $\mathbf{y}$ in the sense of the minimal squared Euclidean distance:

$$\widehat{\mathbf{x}^{(+)}} = \arg \min_{\mathbf{x}^{(+)} \in \mathbf{X}^{(+)}} \left\| \mathbf{y} - \mathbf{x}^{(+)} \right\|^2 . \tag{50}$$

We express the squared Euclidean distance as

$$\left\| \mathbf{y} - \mathbf{x}^{(+)} \right\|^2 = \|\mathbf{y}\|^2 - 2\mathbf{y} \cdot \mathbf{x}^{(+)} + \left\| \mathbf{x}^{(+)} \right\|^2 . \tag{51}$$

Since the first term does not depend on $\mathbf{x}^{(+)}$, (50) is equivalent to

$$\widehat{\mathbf{x}^{(+)}} = \arg \max_{\mathbf{x}^{(+)} \in \mathbf{X}^{(+)}} \left(\mathbf{x}^{(+)} \cdot \mathbf{y} - \frac{1}{2} \left\| \mathbf{x}^{(+)} \right\|^2 \right) . \tag{52}$$

Maximum-likelihood detection can be either performed by an exhaustive search or by tree-based sphere detection. For an exhaustive search, the number of operations is $O(M^{N/2})$ for $N/2$ data symbols. On average, sphere detection is of much less complexity without performance degradation [22], [23]. With suboptimum detection rules, the complexity can be reduced further, which is beyond the scope of this paper, however. We envision two favorable application scenarios for ACO-HCM: (i) harsh environments requiring low data rates ($M = 2$) or (ii) applications seeking low-cost transmitter complexity at arbitrary receiver complexity.

The error event probability depends on the Euclidean distance inside the signal constellation. Recall that δ is the half Euclidean distance for the M-PAM constellation. Let us define

$$\delta \left(\mathbf{X}^{(+)} \right) = \frac{1}{2} \min_{\mathbf{x}_i^{(+)} \neq \mathbf{x}_k^{(+)}} \left\| \mathbf{x}_i^{(+)} - \mathbf{x}_k^{(+)} \right\| \tag{53}$$

as the corresponding quantity for ACO-HCM. Since an analytical evaluation does not seem to be achievable, all distances were calculated numerically. We found $\delta(\mathbf{X}^{(+)}) = \delta$ for all parameters M and N under consideration. This means that the parameter γ in the error event probability of (26) is the same as for the original M-PAM and given by (27). Consequently, the error event probability and, thus, the asymptotic performance remains the same. However, the approximate formula for the bit error probability for M-PAM with Gray mapping is given by [18]

$$P_{\mathrm{b}} \approx \frac{M-1}{\log_2(M) \cdot M} \mathrm{erfc} \left(\sqrt{\frac{3 \log_2 M}{M^2 - 1} \frac{E_{\mathrm{b}}}{N_0}} \right) , \tag{54}$$

where the factor in front results from counting the average number of nearest neighbors inside the constellation. For ACO-HCM, it can not be expected that this number of nearest neighbors remains unchanged, and we obtain

$$P_{\mathrm{b}} \approx C \frac{M-1}{\log_2(M) \cdot M} \mathrm{erfc} \left(\sqrt{\frac{3 \log_2 M}{M^2 - 1} \frac{E_{\mathrm{b}}}{N_0}} \right) \tag{55}$$

with a constant C to incorporate the change. This constant has been evaluated numerically, and the results are listed in Table II. The calculated values are in the range $1 < C < 2$, which means that this constant has no significant influence on the power efficiency.
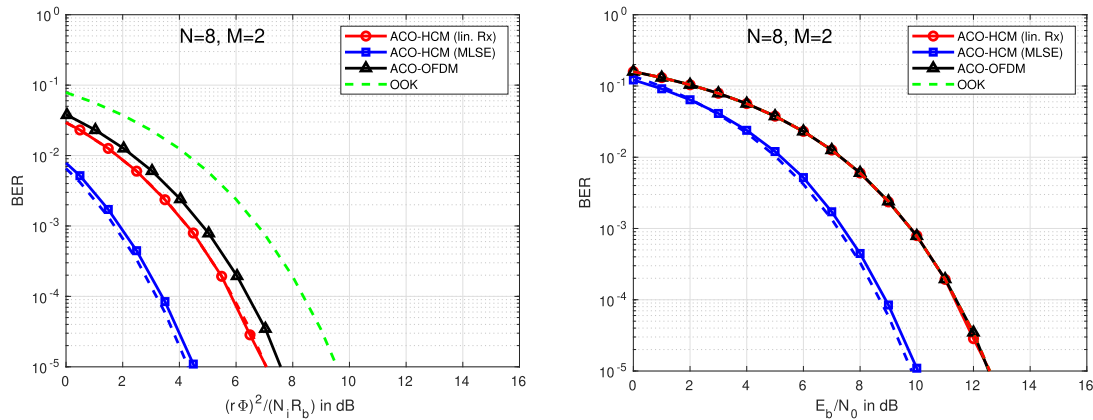
Fig. 4.　BER performance simulations for the optical channel (left) and the electrical channel (right) in comparison with theoretical bit error probabilities (dashed lines) for ACO-HCM/2-PAM for the linear receiver and the MLSE receiver in the absence of time-dispersion. The dashed lines are partially hidden by the solid lines of the same color. For comparison, simulated curves for ACO-OFDM/4-QAM are also shown. The respective theoretical bit error probabilities for OOK [1], [6] in both plots serve as benchmarks.

TABLE II
NUMERICALLY EVALUATED VALUES FOR THE CONSTANT C

$N =$	4	8	16
2-PAM	3/2	7/4	23/16
4-PAM	5/4	43/32	*
8-PAM	9/8	547/445	*

For the optical channel, we write the approximate bit error probability as

$$P_{\mathsf{b}} \approx C \frac{M-1}{\log_2(M) \cdot M} \operatorname{erfc}\left(\sqrt{\frac{3 \log_2 M}{M^2 - 1} \frac{\kappa(r\,\Phi)^2}{N_{\mathsf{i}} R_{\mathsf{b}}}} \right), \quad (56)$$

where κ has to be taken from Table I.

V. BIT ERROR RATE SIMULATIONS FOR THE AWGN CHANNEL

Bit error rate (BER) simulations have been performed for comparison with the theoretical expressions derived above. As an example, Fig. 4 shows simulations for $N = 8$ and $M = 2$ bits per real symbol (ACO-HCM/2-PAM) in comparison with the theoretical curves (drawn as dashed lines). The quantity drawn on the abscissa of the left plot is $10 \log_{10}((r\Phi)^2/(N_{\mathsf{i}} R_{\mathsf{b}}))$. If the decibel difference in terms of optical power is required, it can be obtained by halving the given decibel values on the abscissa. When this is done, 3 dB will indicate a doubling in required optical power. In our presentation, 6 dB on the abscissa means a doubling in required optical power, but for a fixed optical power also a reduction of the bit rate or the noise density to a quarter. The purely electrical quantity E_{b}/N_0 is depicted on the abscissa in the right plot. Both quantities differ by the optical shaping gain factor κ, see (36). The red lines correspond to the linear receiver. The 2 dB gain (red curve in the left plot) for the linear ACO-HCM/2-PAM receiver compared to OOK (green curve) is actually slightly exceeded, as $\kappa \approx 3.56$ is slightly larger than π. Here and in the following, all comparisons of decibel values are taken at BER $= 10^{-5}$. The blue lines correspond to the MLSE receiver as described in Subsection IV-B with the values

for κ and C taken from Tables I and II. For the latter case, a small deviation between theory and simulation can be found. We suspect that this is due to the fact that it is not only the nearest neighbors that are relevant for performance. The MLSE receiver represented by the blue curve provides a further 3 dB asymptotic gain that is not yet fully reached in the BER region shown in the plot. We note that the gain compared to OOK can be interpreted as a coding gain, because this rate-1/2 scheme maps 1 b to 2 chips in contrast to the rate-1 OOK scheme. For comparison, simulated curves for ACO-OFDM with 96 subcarriers and the same number of $M = 2$ bits per real symbol (i.e. ACO-OFDM/4-QAM) are also shown. The small advantage of ACO-HCM with the linear receiver over ACO-OFDM in the left plot is due to the slightly different values for κ. With $\kappa \approx \pi$ [7], ACO-OFDM/4-QAM is almost exactly 2 dB better than OOK. In the electrical channel shown in the right plot, the bit error probability of ACO-HCM/2-PAM with the linear receiver is identical to that of OOK and of ACO-OFDM/4-QAM. In contrast, the same scheme with the MLSE receiver shows the aforementioned 3 dB asymptotic gain that is not yet fully reached in the BER region of the plot.

As a further example, ACO-HCM/4-PAM is considered, which has the same rate as OOK, i.e., one bit per chip. The results are shown in Fig. 5. Whilst the linear receiver performs 2 dB worse than OOK in the optical channel (left plot), ACO-HCM with the MLSE receiver still provides a 1 dB gain compared to OOK for this scheme without any rate loss. For comparison, simulated curves for ACO-OFDM with 96 subcarriers and the same number of $M = 4$ bits per real symbol (i.e. ACO-OFDM/16-QAM) are also shown. It can be observed that ACO-OFDM/16-QAM has approximately the same performance as ACO-HCM/4-PAM with linear detection. This can be expected because both schemes have the same gain factor $\kappa \approx \pi$, see Table I. Thus, ACO-HCM/4-PAM with ML detection outperforms ACO-OFDM/16-QAM by 3 dB. Classical 4-ASK (i.e. 4-PAM with DC offset) performs approximately 4 dB worse than ACO-OFDM/16-QAM in the optical channel, see Fig. 4 in [7]. The same figure shows that HCM performs even worse than classical 4-ASK.
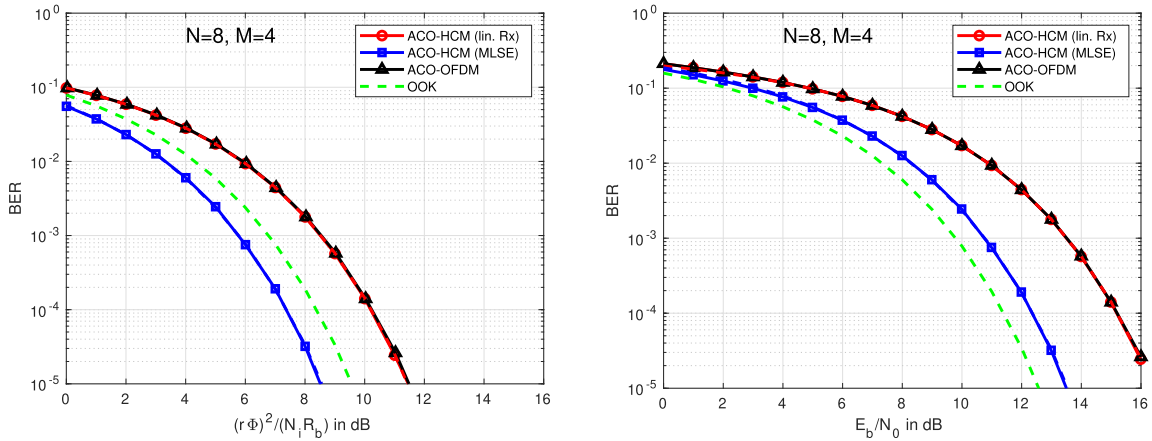
Fig. 5. BER performance simulations for the optical channel (left) and the electrical channel (right) in comparison with theoretical bit error probabilities (dashed lines) for ACO-HCM/4-PAM for the linear receiver and the MLSE receiver in the absence of time-dispersion. The dashed lines are partially hidden by the solid lines of the same color. For comparison, simulated curves for ACO-OFDM/16-QAM are also shown. The respective theoretical bit error probabilities for OOK [1], [6] in both plots serve as benchmarks.

VI. PERFORMANCE IN A TIME-DISPERSIVE OPTICAL CHANNEL

A. Channel Model and Receiver Structure

For a time-dispersive optical channel, (31) has to be replaced by

$$y(t) = h(t) * x(t) + n(t),\qquad(57)$$

where the (deterministic) impulse response $h(t)$ characterizes the time-dispersion of the channel. Time-dispersion is due to multipath propagation and/or the finite bandwidth of the light source. The optical received power (without noise) is proportional to

$$\mathrm{E}\{h(t) * x(t)\} = H(0)\,\mathrm{E}\{x(t)\},\qquad(58)$$

where the channel frequency response $H(f)$ is the Fourier transform of $h(t)$. It is convenient to include the optical path loss in the signal $x(t)$ and normalize the frequency response as

$$H(0) = \int_0^\infty h(t)\,\mathrm{d}t = 1.\qquad(59)$$

An appropriate receiver must take the time-dispersion into account. Let us first consider the case that only a single ACO-HCM signal vector $\mathbf{x}^{(+)}$ is transmitted. Each possible discrete symbol vector $\mathbf{x}^{(+)} \in \mathbf{X}^{(+)}$ uniquely corresponds to a continuous signal vector $x^{(+)}(t)$ that is transmitted though the dispersive channel given by (57). The MLSE in (52) has to be replaced by

$$\widehat{\mathbf{x}^{(+)}} = \arg\max_{\mathbf{x}^{(+)}\in\mathbf{X}^{(+)}} \mu_y\left(\mathbf{x}^{(+)}\right)\qquad(60)$$

with

$$\mu_y\left(\mathbf{x}^{(+)}\right) = \int_0^\infty \left(h(t) * x^{(+)}(t)\right) y(t)\,\mathrm{d}t$$
$$-\frac{1}{2}\int_0^\infty \left(x^{(+)}(t)\right)^2 \mathrm{d}t.\qquad(61)$$

For a sequence of signal vectors, the receiver has to cope with inter-symbol interference (ISI) between successive signal vectors. In order to keep the receiver simple, only decisions on single symbol vectors are performed, and the upper integral limit in the above equation is set to the symbol period $T_\mathsf{s} = NT_\mathsf{c}$, where T_c is the chip period:

$$\mu_y\left(\mathbf{x}^{(+)}\right) = \int_0^{T_\mathsf{s}} \left(h(t) * x^{(+)}(t)\right) y(t)\,\mathrm{d}t$$
$$-\frac{1}{2}\int_0^{T_\mathsf{s}} \left(x^{(+)}(t)\right)^2 \mathrm{d}t.\qquad(62)$$

This MLSE detection rule is applied to every symbol period of length T_s.

In order to reduce the ISI, we may introduce an empty *guard chip* of length T_g at the end of each symbol, which means that the symbol period is extended to $T_\mathsf{s} = NT_\mathsf{c} + T_\mathsf{g}$, and the MLSE detector in (62) works with this extended symbol period. This guard chip sacrifices data rate, but no energy. In the simplest case, one may choose $T_\mathsf{g} = T_\mathsf{c}$, which extends the symbol period to $T_\mathsf{s} = (N + 1)T_\mathsf{c}$ and reduces the bit rate by the factor $N/(N + 1)$ to $R_\mathsf{b} = \frac{N}{2(N+1)}\log_2(M)R_\mathsf{c}$. The guard chip in ACO-HCM is the analog to single-tap equalization in combination with a cyclic prefix in (ACO-)OFDM, with the difference that the empty guard chip is appended in the time domain to reduce ISI, while single-tap equalization takes place in the frequency domain. The length of the guard chip is adjustable by multiples of T_c, like the length of the cyclic prefix in (ACO-)OFDM. Therefore, with exhaustive search the complexity is still $O(M^{N/2})$ if the channel is dispersive.

B. Bit Error Rate Simulations for the Dispersive Channel

A popular model for the time-dispersive optical channel is characterized by the exponential impulse response [24], [25], [26]

$$h(t) = \frac{1}{\tau}e^{-t/\tau}\Theta(t),\qquad(63)$$

where the time constant τ characterizes the dispersion of the channel. The corresponding frequency response

$$H(f) = \frac{1}{1 + j2\pi f\tau}\qquad(64)$$

belongs to a low-pass filter with 3 dB bandwidth

$$f_{3\,\mathrm{dB}} = \frac{1}{2\pi\tau}\,. \tag{65}$$

1) ACO-OFDM System Parameters: As a reference for performance comparison, we consider an ACO-OFDM/4-QAM system [7], [26], [27] with subcarrier positions that just fill this 3 dB bandwidth. For a time-discrete simulation, it must be ensured that sufficient number of samples lie within the time constant τ. This means that the sampling frequency f_{s} must be much higher than $f_{3\,\mathrm{dB}}$. We choose

$$f_{\mathsf{s}}\tau = 10\,, \tag{66}$$

i.e. ten samples inside τ, which leads to $f_{\mathsf{s}} = 10 \cdot 2\pi f_{3\,\mathrm{dB}}$. $10\times$ oversampling is reasonable to ensure sufficient accuracy and is consistent with the literature, see e.g. [26]. This high oversampling is only needed for a proper emulation of the dispersive channel in computer-based simulations rather than for a practical implementation of ACO-HCM. A suitable solution of oversampling in the time domain is zero padding in the frequency domain. In this way, the FFT length N_{FFT} is chosen to be much larger than the number K of modulated subcarriers inside the 3 dB bandwidth. For $N_{\mathsf{FFT}} = 2048$ and (66), there are just $K = 16$ modulated subcarriers inside the 3 dB bandwidth. For a symbol duration T, the bit rate is given by

$$R_{\mathsf{b}} = \frac{2\,K}{T} = \frac{2\,K}{N_{\mathsf{FFT}}} f_{\mathsf{s}}\,. \tag{67}$$

With the parameters given above, this results in

$$R_{\mathsf{b}}/f_{3\,\mathrm{dB}} = 0.98\,\mathrm{bit/s/Hz}\,. \tag{68}$$

As we shall see below, a cyclic prefix of eight samples is sufficient for this channel, and the reduction of the data rate due to the cyclic prefix can thus be neglected.

2) ACO-HCM System Parameters: To obtain an ACO-HCM/2-PAM system parameter set with approximately the same normalized data rate as given by (68), we choose a chip period

$$T_{\mathsf{c}} = \frac{25}{9}\tau\,. \tag{69}$$

For $N = 8$ and $T_{\mathsf{g}} = T_{\mathsf{c}}$, the bit rate is

$$R_{\mathsf{b}} = \frac{1}{2T_{\mathsf{c}}} \cdot \frac{8}{9}\,, \tag{70}$$

which results in

$$R_{\mathsf{b}}/f_{3\,\mathrm{dB}} = 1.01\,\mathrm{bit/s/Hz}\,. \tag{71}$$

The frequency response of the channel with these parameters is shown in Fig. 6 together with the ACO-HCM spectrum before (Tx) and after (Rx) the dispersive channel. A significant distortion of the useful spectrum can be observed. The ACO-OFDM subcarrier positions are marked as circles.

The ACO-HCM time signal before and after the dispersive channel is shown in Fig. 7. The absorption of the time dispersion by the guard chip can be clearly observed at the end of the 1st, 3rd, and 5th symbol interval. The guard chip reduces reverberation into the next symbol.
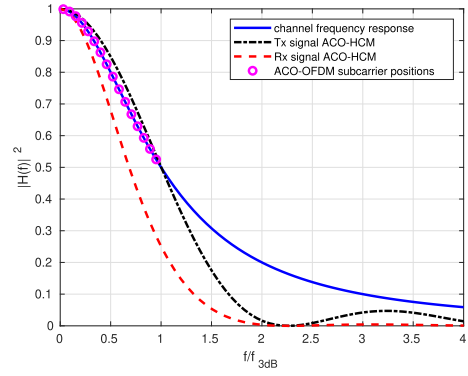

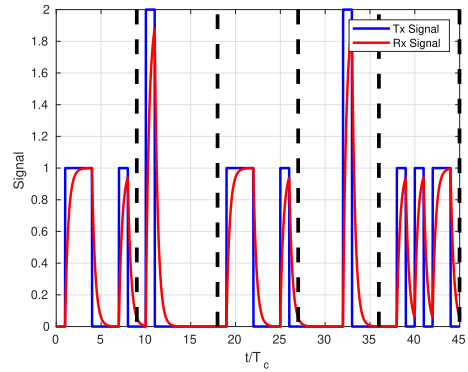Fig. 6.　Frequency response of the dispersive channel and spectra of the signals.

Fig. 7.　ACH-HCM time signal before and after the dispersive channel. Each symbol consists of eight useful chips plus an empty guard chip. The dashed lines indicate the boundaries between adjacent symbols of length $9T_{\mathsf{c}}$. The guard chip reduces ISI.
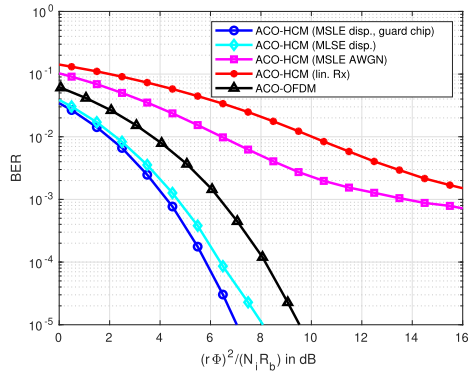

Fig. 8.　Bit error rate simulations for ACH-HCM/2-PAM and ACO-OFDM/4-PAM in the time-dispersive optical channel shown in Fig. 6.

3) Bit Error Rate Simulations for a Time-Dispersive Channel: Bit error rate simulations were performed for ACO-HCM/2-PAM compared to ACO-OFDM/4-QAM in the time-dispersive optical channel with the parameters shown above. The results are shown in Fig. 8. At BER $= 10^{-5}$ and the same bit rate, we observe a 2.5 dB performance gain for ACO-HCM/2-PAM with guard chip (blue curve) compared to ACO-OFDM/4-QAM (black curve). The losses compared to the AWGN channel are about 2.5 dB for ACO-HCM/2-PAM and 2 dB for ACO-OFDM/4-QAM, respectively. It should be noted

that for ACO-OFDM, these losses can be fully explained by the low-pass characteristics of the channel. Different OFDM cyclic prefix lengths were investigated, and we found that a rather short cyclic prefix of eight samples is sufficient for $N_{\mathsf{FFT}} = 2048$ and $f_{\mathsf{s}}\tau = 10$.

Omitting the ACO-HCM guard chip (see the cyan curve in Fig. 8) leads to a loss of approximately $1\,\mathrm{dB}$, but the performance is still better than for ACO-OFDM. However, it is highly recommended for ACO-HCM to use an MLSE receiver that is matched to the given dispersive channel, or a reduced-complexity nonlinear receiver taking the channel dispersion into account. With the MLSE receiver designed for the AWGN channel (magenta curve in Fig. 8), an acceptable BER cannot be reached. As expected, the linear receiver (red curve) performs even worse.

VII. EXTENSIONS

The ACO-HCM concept can be extended in various directions. Some possible extensions are briefly outlined next.

Unfortunately, ACO-OFDM, PAM-DMT, and Flip-OFDM suffer from a rate loss compared to DCO-OFDM, because one signal dimension is wasted. Spectral efficiency can be improved by so-called spectrally-enhanced unipolar OFDM techniques [28]. The roots of enhanced and layered methods have been established in [29] by proposing successive decoding of anti-periodic OFDM signals. Specific methods include layered ACO-OFDM (LACO-OFDM) [30], enhanced ACO-OFDM (eACO-OFDM) [31], and enhanced PAM-DMT (ePAM-DMT) [32]. A comparison of these and further methods was recently presented in [28].

- In LACO-OFDM, the subcarriers are divided into different layers and modulated by different kinds of ACO-OFDM, which are combined for simultaneous transmission [30]. This principle can also be applied to the Hadamard transform: the Hadamard matrix can be divided into different layers (i.e., submatrices) that are modulated by different dimensions of ACO-HCM, which are finally combined for simultaneous transmission. We call this novel scheme LACO-HCM.
- In eACO-OFDM, parallel data streams are first ACO-OFDM modulated, then processed, and finally superimposed in order to close the spectral gap with respect to DCO-OFDM [31]. By replacing ACO-OFDM with ACO-HCM in the first step, a novel modulation scheme dubbed eACO-HCM is obtained.
- ePAM-DMT was proposed as a solution to fill the spectral gap between PAM-DMT and DCO-OFDM [32]. This was achieved by allowing multiple streams of PAM-DMT to be superimposed and successively demodulated at the receiver side. This concept can be applied to ACO-HCM as well, since PAM-DMT is an integral part of ACO-HCM.

Hybrid methods are another option. For example, hybrid asymmetrically clipped optical OFDM (HACO-OFDM) uses ACO-OFDM on the odd subcarriers and PAM-DMT on the even subcarriers to improve the bandwidth efficiency of ACO-OFDM and PAM-DMT, respectively [33]. Along the same lines,

ACO-HCM may be combined with PAM-DMT. It would be interesting to explore similar ideas to ACO-HCM in future work.

So far, ACO-HCM has been treated as a modulation technique, but it can also be used for multiplexing. Due to its inherent spreading, ACO-HCM can further be considered as a multiuser scheme (ACO-HCMA), similar to synchronous DS-CDMA. For this purpose, the set of Hadamard sequences can be assigned to different users on the downlink.

ACO-HCM is well suited in conjunction with the spatial summation architecture [34], [35]. In this topology, different layers are transmitted via different light sources. The superposition takes place in the medium.

VIII. CONCLUSION

In this paper, a new intensity modulation scheme called ACO-HCM is proposed and investigated. This modulation scheme combines the concepts of ACO-OFDM and HCM and is suitable for a large variety of optical wireless communication (OWC) applications. The waveform design exploits the inherent properties of Hadamard codes. For a linear receiver, which is similar to the decorrelation receiver known for DS-CDMA, the error rate is calculated in closed form for the AWGN channel. Towards this goal, the waveform-dependent shaping gain factor κ is calculated. This parameter is a measure of amplitude fluctuations and related to, but different, from the PAPR. The PAPR of ACO-HCM is derived analytically for the electrical and the optical domain in closed form. Remarkably, in optical intensity modulation schemes, a maximization of κ improves the power efficiency of the optical modulation scheme given the same received power in the optical domain. It is shown that the squared PAPR in the optical domain is proportional to the PAPR in the electrical domain, and the constant of proportionality is equal to κ. This law holds for all optical IM/DD digital modulation schemes. We argue that precoding-type PAPR reduction techniques are counter-productive as long as nonlinear effects of the light source are avoidable. In the case of ACO-HCM the latter is indeed the case, because the transmit signal is discrete-valued. Besides the linear receiver, the optimal receiver in the sense of MLSE is derived. This receiver provides an additional gain of approximately 3 dB on the AWGN channel. Furthermore, the MLSE receiver has been extended to the case of a dispersive channel. In the presence of channel dispersion, MLSE detection matched to the channel is recommendable and provides promising performance results. Also, it is shown that ACO-HCM outperforms ACO-OFDM in the presence of time dispersion given the same bit rate. Finally, possible extensions are suggested, most of which are the subject of future elaborations. Experimental verification of an ACO-HCM-based underwater OWC modem is the subject of ongoing work.

APPENDIX A
DERIVATION OF PEAK-TO-AVERAGE POWER RATIO OF ACO-HCM

In this appendix, the PAPR of ACO-HCM is derived for the electrical domain and the optical domain, respectively. Also, a comparison with OOK is presented.

From (14) and (17) it follows that the elements $x_m^{(+)}$ of the clipped ACO-HCM signal vector $\mathbf{x}^{(+)}$ take on values between zero and

$$x_{\max}^{(+)} = (M - 1)\sqrt{\frac{N}{2}}\delta. \tag{72}$$

We further note that due to the isometry (12) and the normalization included in the clipping, all vectors have the same energy

$$\|\mathbf{u}\|^2 = \|\mathbf{x}\|^2 = \left\|\mathbf{x}^{(+)}\right\|^2. \tag{73}$$

Since $N/2$ PAM symbols are mapped onto N chips, the average energy per chip is given by

$$\mathrm{E}\left\{\left(x_m^{(+)}\right)^2\right\} = \frac{1}{2}\mathrm{E}\{u_n^2\} \stackrel{[18]}{=} \frac{\delta^2}{6}(M^2 - 1). \tag{74}$$

Hence, combining (72) and (74) yields

$$\frac{\left(x_{\max}^{(+)}\right)^2}{\mathrm{E}\left\{\left(x_i^{(+)}\right)^2\right\}} = \frac{(M-1)^2 \frac{N}{2}\delta^2}{\frac{\delta^2}{6}(M^2-1)} = 3N\frac{M-1}{M+1}. \tag{75}$$

This is the PAPR in the electrical domain, or electrical PAPR for short:

$$\mathrm{PAPR}_{\mathrm{el}} = \frac{\left(x_{\max}^{(+)}\right)^2}{\mathrm{E}\left\{\left(x_i^{(+)}\right)^2\right\}} = 3N\frac{M-1}{M+1}. \tag{76}$$

Let us define the PAPR in the optical domain as the ratio

$$\mathrm{PAPR}_{\mathrm{opt}} = \frac{x_{\max}^{(+)}}{\mathrm{E}\left\{x_i^{(+)}\right\}} \tag{77}$$

between the maximal and the average optical power. It is interesting to note that the optical PAPR is related to the electrical PAPR of (76) by the parameter κ according to

$$\mathrm{PAPR}_{\mathrm{opt}}^2 = \frac{\left(x_{\max}^{(+)}\right)^2}{\mathrm{E}\left\{\left(x_i^{(+)}\right)\right\}^2}$$

$$= \frac{\left(x_{\max}^{(+)}\right)^2}{\mathrm{E}\left\{\left(x_i^{(+)}\right)^2\right\}} \frac{\mathrm{E}\left\{\left(x_i^{(+)}\right)^2\right\}}{\mathrm{E}\left\{\left(x_i^{(+)}\right)\right\}^2}$$

$$= \mathrm{PAPR}_{\mathrm{el}} \cdot \kappa \tag{78}$$

or

$$\kappa = \frac{\mathrm{PAPR}_{\mathrm{opt}}^2}{\mathrm{PAPR}_{\mathrm{el}}}. \tag{79}$$

As a benchmark, let us compare the PAPR of ACO-HCM with the PAPR of OOK. For the special case of NRZ-OOK,

$$x_{\max} = 2\delta, \quad \mathrm{E}\left\{x(t)\right\} = \delta, \text{ and } \mathrm{E}\left\{x^2(t)\right\} = 2\delta^2. \tag{80}$$

Therefore,

$$\mathrm{PAPR}_{\mathrm{opt}} = 2 \text{ and } \mathrm{PAPR}_{\mathrm{el}} = 2 \tag{81}$$

and hence

$$\frac{\mathrm{PAPR}_{\mathrm{opt}}^2}{\mathrm{PAPR}_{\mathrm{el}}} = 2 = \kappa. \tag{82}$$

As opposed to the fixed PAPR of OOK, for ACO-HCM $\mathrm{PAPR}_{\mathrm{el}}$ is between N (for $M = 2$) and $3N$ (for large M).

APPENDIX B
PROOF OF THEOREM 1

We express (15) as

$$u_n = \sum_{m=1}^{N} g_n[m]x[m] \tag{83}$$

and recall that $g_n[\cdot]$ and $x[\cdot]$ are signals of odd symmetry, i.e.

$$g_n[N - (m - 1)] = -g_n[m] \tag{84}$$

and

$$x[N - (m - 1)] = -x[m]. \tag{85}$$

Splitting up the sum in (83) and using these properties, we find

$$u_n = \sum_{m=1}^{N/2} g_n[m]x[m] + \sum_{m=N/2+1}^{N} g_n[m]x[m]$$

$$= \sum_{m=1}^{N/2} g_n[m]x[m] + \sum_{m=1}^{N/2} g_n[N - (m - 1)]x[N - (m - 1)]$$

$$= \sum_{m=1}^{N/2} g_n[m]x[m] + \sum_{m=1}^{N/2} g_n[m]x[m].$$

This yields

$$u_n = 2\sum_{m=1}^{N/2} g_n[m]x[m], \tag{86}$$

i.e., as an immediate consequence of the odd symmetry of the base vectors, the first half of the signal $x[n]$ already determines the symbols u_n.

We now rewrite $x^{(+)}[m] = x_n^{(+)}$ for the clipped signal. The signal $x[m]$ can be uniquely decomposed into its non-negative part and its non-positive part according to

$$x[m] = \frac{1}{\sqrt{2}}\left(x^{(+)}[m] + x^{(-)}[m]\right) \tag{87}$$

where $x^{(-)}[m]$ is defined just by the above equation. Recall that the factor $1/\sqrt{2}$ serves to retain the energy when clipping the signal. As a direct consequence of (85) and (87), we obtain the properties

$$x^{(+)}[N - (m - 1)] = -x^{(-)}[m] \tag{88}$$

and

$$x^{(-)}[N - (m - 1)] = -x^{(+)}[m]. \tag{89}$$

We now write (21) as

$$u_n^{(+)} = \sum_{m=1}^{N} g_n[m]x^{(+)}[m] \,, \tag{90}$$

split up the sum, and use (84) and (88) to obtain

$$u_n^{(+)} = \sum_{m=1}^{N/2} g_n[m]x^{(+)}[m] + \sum_{m=N/2+1}^{N} g_n[m]x^{(+)}[m]$$

$$= \sum_{m=1}^{N/2} g_n[m]x^{(+)}[m]$$

$$+ \sum_{m=1}^{N/2} g_n[N-(m-1)]x^{(+)}[N-(m-1)]$$

$$= \sum_{m=1}^{N/2} g_n[m]x^{(+)}[m] + \sum_{m=1}^{N/2} g_n[m]x^{(-)}[m]$$

$$= \sum_{m=1}^{N/2} g_n[m]\left(x^{(+)}[m] + x^{(-)}[m]\right) \,. \tag{91}$$

With (87), this yields

$$u_n^{(+)} = \sqrt{2} \sum_{m=1}^{N/2} g_n[m]x[m] \,. \tag{92}$$

Comparing (92) with (86) we obtain the desired result

$$u_n^{(+)} = \frac{1}{\sqrt{2}} u_n$$

stated in Theorem 1.

ACKNOWLEDGMENT

REFERENCES

[1] J. R. Barry, *Wireless Infrared Communications*. Alphen aan den Rijn, The Netherlands: Kluwer, 1994.

[2] J. M. Kahn and J. R. Barry, "Wireless infrared communications," *Proc. IEEE*, vol. 85, no. 2, pp. 265–298, Feb. 1997.

[3] S. Arnon, *Visible Light Communication*. Cambridge, U.K.: Cambridge Univ. Press, 2015.

[4] S. Dimitrov and H. Haas, *Principles of LED Light Communications: Towards Networked Li-Fi*. Cambridge, U.K.: Cambridge Univ. Press, 2015.

[5] Z. Ghassemlooy, L. N. Alves, S. Zvanovec, and M. A. Khalighi, *Visible Light Communications: Theory and Applications*. Boca Raton, FL, USA: CRC Press, 2017.

[6] P. A. Hoeher, *Visible Light Communications: Theoretical and Practical Foundations*. Munich, Germany: Carl Hanser, 2019.

[7] H. Schulze and P. A. Hoeher, "On the general error event probability evaluation of optical intensity modulation schemes," *IEEE Photon. J.*, vol. 14, no. 5, pp. 1–8, Oct. 2022, Art. no. 7954008.

[8] J. B. Carruthers and J. M. Kahn, "Multiple-subcarrier modulation for nondirected wireless infrared communication," *IEEE J. Sel. Areas Commun.*, vol. 14, no. 3, pp. 538–546, Apr. 1996.

[9] O. González, R. Pérez-Jiménez, S. Rodriguez, J. Rabadán, and A. Ayala, "OFDM over indoor wireless optical channel," *IEE Proc.-Optoelectron.*, vol. 152, no. 4, pp. 199–204, Aug. 2005.

[10] J. Armstrong and A. J. Lowery, "Power efficient optical OFDM," *Electron. Lett.*, vol. 42, no. 6, pp. 370–372, 2006.

[11] J. Armstrong and B. J. C. Schmidt, "Comparison of asymmetrically clipped optical OFDM and DC-biased optical OFDM in AWGN," *IEEE Commun. Lett.*, vol. 12, no. 5, pp. 343–345, May 2008.

[12] S. C. J. Lee, S. Randel, F. Breyer, and A. M. J. Koonen, "PAM-DMT for intensity-modulated and direct detection optical communication systems," *IEEE Photon. Technol. Lett.*, vol. 21, no. 23, pp. 1749–1751, Dec. 2009.

[13] N. Fernando, Y. Hong, and E. Viterbo, "Flip-OFDM for unipolar communication systems," *IEEE Trans. Commun.*, vol. 60, no. 12, pp. 3726–3733, Dec. 2012.

[14] S. D. Dissanayake and J. Armstrong, "Comparison of ACO-OFDM, DCO-OFDM and ADO-OFDM in IM/DD systems," *IEEE/OSA J. Lightw. Technol.*, vol. 31, no. 7, pp. 1063–1072, Apr. 2013.

[15] M. Noshad and M. Brandt-Pearce, "Hadamard coded modulation: An alternative to OFDM for wireless optical communications," in *Proc. IEEE Glob. Commun. Conf.*, 2014, pp. 2102–2107.

[16] M. Noshad and M. Brandt-Pearce, "Hadamard-coded modulation for visible light communications," *IEEE Trans. Commun.*, vol. 64, no. 3, pp. 1167–1175, Mar. 2016.

[17] J. Lian, M. Noshad, and M. Brandt-Pearce, "Indoor multiuser visible light communication systems using Hadamard-coded modulation," *Philos. Trans. Roy. Soc. A*, vol. 378, 2020, Art. no. 20190183.

[18] J. Proakis and M. Salehi, *Digital Communications*. 5th ed.New York, NY, USA: McGraw-Hill, 2008.

[19] T. Matsuda, A. Naka, and S. Saito, "Comparison between NRZ and RZ signal formats for in-line amplifier transmission in the zero-dispersion regime," *OSA J. Lightw. Technol.*, vol. 16, no. 3, pp. 340–348, Mar. 1998.

[20] H. G. Myung, J. Lim, and D. J. Goodman, "Single carrier FDMA for uplink wireless transmission," *IEEE Veh. Technol. Mag.*, vol. 1, no. 3, pp. 30–38, Sep. 2006.

[21] M. Park, H. Jun, J. Cho, N. Cho, D. Hong, and C. Kang, "PAPR reduction in OFDM transmission using Hadamard transform," in *Proc. IEEE Int. Conf. Commun.*, 2000, pp. 430–433.

[22] J. Jaldén and B. Ottersten, "On the complexity of sphere decoding in digital communications," *IEEE Trans. Signal Process.*, vol. 53, no. 4, pp. 1474–1484, Apr. 2005.

[23] B. Hassibi and H. Vikalo, "On the sphere-decoding algorithm I. Expected complexity," *IEEE Trans. Signal Process.*, vol. 53, no. 8, pp. 2806–2818, Aug. 2005.

[24] J. B. Carruthers and J. M. Kahn, "Modeling of nondirected wireless infrared channels," *IEEE Trans. Commun.*, vol. 45, no. 10, pp. 1260–1268, Oct. 1997.

[25] V. Jungnickel, V. Pohl, S. Nönnig, and C. von Helmolt, "A physical model of the wireless infrared communication channel," *IEEE J. Sel. Areas Commun.*, vol. 20, no. 3, pp. 631–640, Apr. 2002.

[26] S. K. Wilson and J. Armstrong, "Transmitter and receiver methods for improving asymmetrically-clipped optical OFDM," *IEEE Trans. Wireless Commun.*, vol. 8, no. 9, pp. 4561–4567, Sep. 2009.

[27] J. Armstrong, B. J. Schmidt, D. Kalra, H. A. Suraweera, and A. J. Lowery, "Performance of asymmetrically clipped optical OFDM in AWGN for an intensity modulated direct detection system," in *Proc. IEEE Glob. Commun. Conf.*, 2006, pp. 1–5.

[28] X. Zhang, Z. Babar, P. Petropoulos, H. Haas, and L. Hanzo, "The evolution of optical OFDM," *IEEE Commun. Surveys Tuts.*, vol. 23, no. 3, pp. 1430–1457, Jul.–Sep. 2021.

[29] L. Chen, B. Krongold, and J. Evans, "Successive decoding of anti-periodic OFDM signals in IM/DD optical channel," in *Proc. IEEE Int. Conf. Commun.*, 2010, pp. 1–6.

[30] Q. Wang, C. Qian, X. Guo, Z. Wang, D. G. Cunningham, and I. H. White, "Layered ACO-OFDM for intensity-modulated direct-detection optical wireless transmission," *Opt. Exp.*, vol. 23, no. 9, pp. 12382–12393, May 2015.

[31] M. S. Islim, D. Tsonev, and H. Haas, "On the superposition modulation for OFDM-based optical wireless communication," in *Proc. IEEE GlobalSIP*, 2015, pp. 1022–1026.

[32] M. S. Islim and H. Haas, "Augmenting the spectral efficiency of enhanced PAM-DMT-based optical wireless communications," *Opt. Expr.*, vol. 24, no. 11, pp. 11932–11949, 2016.

[33] B. Ranjha and M. Kavehrad, "Hybrid asymmetrically clipped OFDM-based IM/DD optical wireless system," *IEEE/OSA J. Opt. Commun. Netw.*, vol. 6, no. 4, pp. 387–396, Apr. 2014.

[34] M. S. Mossaad, S. Hranilovic, and L. Lampe, "Visible light communications using OFDM and multiple LEDs," *IEEE Trans. Commun.*, vol. 63, no. 11, pp. 4304–4313, Nov. 2015.

[35] G. J. M. Forkel and P. A. Hoeher, "Constrained intensity superposition: A hardware-friendly modulation method," *IEEE/OSA J. Lightw. Technol.*, vol. 36, no. 3, pp. 658–665, Feb. 2018.